Supplementary Information for Optimal Design and Integration of Decentralized Electrochemical Energy Storage with Renewables and Fossil Plants

Manali S. Zantye[1], Akhilesh Gandhi[1], Yifan Wang[2], Sai Pushpitha Vudata[2], Debangsu Bhattacharyya[2], M. M. Faruque Hasan[1*]

[1]Artie McFerrin Department of Chemical Engineering, Texas A&M University
College Station, TX 77843-3122, USA.

[2]Department of Chemical and Biomedical Engineering, West Virginia University
Morgantown, WV 26506, USA.

Contents

S1 NaS Battery Model Derivation and Validation

The detailed models from Schaefer et al.[1] form the basis of the reduced-order models of the NaS battery developed in this work. The aforementioned work extensively considers the thermo-electrochemical cell phenomena for studying the dynamic operation of the cell under load-following conditions. The influence of the SOD on the cell EMF is studied through the modeling of electrochemical cell reactions using Arrhenius-type rate equations with temperature-dependent terms. In addition, species as well as energy conservation is modeled for the chemical and ionic species of the sulfur electrode, beta"-alumina electrolyte and sodium electrode depending on the SOD. The resulting coupled system of partial differential equations (PDEs) is solved using Aspen Custom Modeler V.8.4 and validated with experimental data. The data obtained on simulating the dynamic profiles is used to develop the battery reduced-order models using the NAARX (nonlinear additive autoregressive with exogenous input)-based approach.

The NAARX-based reduced models, with the general form represented by Eq. 1, use nonlinear functions of the previously observed outputs and an exogenous input time-series u to determine the output y at any time instant t:

$$y_t = \sum_{i=0}^{n} H_1(i,p) u_{t-i}^{p} + \sum_{j=1}^{r} H_2(j,q) y_{t-j}^{q},\ p = 1:P, q = 1:Q. \tag{1}$$

Here, H_1 and H_2 denote the parameter vectors determined based on the least square estimate considering a linear in parameter (LIP) model:

$$\begin{aligned} y_t &= \psi_t H, \\ H &= (\psi^{\mathrm{T}}\psi)^{-1}\psi^{\mathrm{T}} Y, \end{aligned} \tag{2}$$

where, ψ represents the regression vector and Y represents the output vector, which are obtained using the simulation data. The criterion for model selection is Akaike information criterion (AIC), which is a well-accepted information-theoretic criterion for selecting the best approximating model from a set of candidate models for a given set of data. It rewards the goodness of fit as well as penalizes the increased number of estimated parameters, thereby reducing overfitting. AIC is given by:

$$AIC = N \ln\left(\frac{TSE}{N}\right) + 2K, \tag{3}$$

where, N denotes the number of data points, TSE represents the total squared error and K is the number of fitted parameters. Model complexity is increased until the AIC value changes significantly. Once no significant change in AIC value is observed, the simpler model is chosen. Using this procedure, the input memory n, output memory r and exponent values P and Q are determined from the model which exhibits a good trade-off between model simplicity and goodness of fit.

The reduced-order models for the NaS cell are generated in MATLAB with the inputs u as the state of discharge of the cell SOD^{cell} (%) and the value of the current through the cell I^{cell} (ampere). The output y includes the cell voltage V^{cell} (volt). We define the following set mappings for representation of the reduced-order models: Set mapping $map^{s1}_{s,is,is1}$ links the individual states $is, is1$ to their combination $s \in S$, with $map^{s1}_{s,is,is1} = 1$ for the following values of $\{s, is, is1\}$: $\{1c, single, charge\}$, $\{1d, single, discharge\}$, $\{2c, two, charge\}$, $\{2d, two, discharge\}$. We further define the following sets for representation of the NAARX-based dynamic model: sets $\mathcal{Z}, \mathcal{A}, \mathcal{L}$ denote the set of exponents of the first and second exogenous input time series and the output time series respectively with $z \in \mathcal{Z} = \{1\}, a \in \mathcal{A} = \{1\}, l \in \mathcal{L} = \{1\}$. Sets $\mathcal{J}, \mathcal{B}, \mathcal{G}$ indicate the set of the number of past values to be considered for the first input series, second input series and the output time series respectively with $j \in \mathcal{J} = \{1, 2, 3\}, b \in \mathcal{B} = \{1, 2, 3\}, g \in \mathcal{G} = \{1, 2\}$. The index $k \in \mathcal{K} = \{1, 2, 3, 4, 5\}$ signifies the terms of the parameter vector H_s to be multiplied with the input and output series in the NAARX model for state s.

Additionally, we introduce set mappings $map^{p1}_{s,z}, map^{p2}_{s,a}, map^{q1}_{s,l}$ to indicate the exponents z, a and l which will be active for the dynamic model of state s. The following equations represent this:

$$map^{p1}_{s,z} = 1, \qquad \forall z \leq p1_s, \tag{4a}$$

$$map^{p2}_{s,a} = 1, \qquad \forall a \leq p2_s, \tag{4b}$$

$$map^{q1}_{s,l} = 1, \qquad \forall l \leq q1_s. \tag{4c}$$

Similarly, set mappings $map^{n1}_{s,j}, map^{n2}_{s,b}, map^{r1}_{s,g}$ denote the number of past values of the time series used for prediction of the present battery output for state s. Here, we define:

$$map^{n1}_{s,j} = 1, \qquad \forall j \leq n1_s, \tag{5a}$$

$$map^{n2}_{s,b} = 1, \qquad \forall b \leq n2_s, \tag{5b}$$

$$map^{r1}_{s,g} = 1, \qquad \forall g \leq r1_s. \tag{5c}$$

Mappings $map^{k1}_{s,k,z,j}, map^{k2}_{s,k,a,b}, map^{k3}_{s,k,l,g}$ link the elements of set K to state s, given by the following:

$$map^{k1}_{s,k,z,j} = 1, \qquad \forall z \leq p1_s, j \leq n1_s, k = (z-1)n1_s + j, \tag{6a}$$

$$map^{k2}_{s,k,a,b} = 1, \qquad \forall a \leq p2_s, b \leq n2_s, k = n1_s p1_s + (a-1)n2_s + b, \tag{6b}$$

$$map^{k3}_{s,k,l,g} = 1, \qquad \forall l \leq q1_s, g \leq r1_s, k = n1_s p1_s + n2_s p2_s + (l-1)r1_s + g. \tag{6c}$$

The values of the parameters $p1_s, p2_s, q1_s, n1_s, n2_s, r1_s$ and $H_{s,k}$ for state $s \in \mathcal{S}$ are given in Table S1.

Table S1: NaS cell surrogate model parameters

Parameter	Value	Parameter	Value	Parameter	Value
$p1_{1c}$	1	$p2_{1c}$	1	$q1_{1c}$	1
$p1_{1d}$	1	$p2_{1d}$	1	$q1_{1d}$	1
$p1_{2c}$	1	$p2_{2c}$	1	$q1_{2c}$	1
$p1_{2d}$	1	$p2_{2d}$	1	$q1_{2d}$	1
$n1_{1c}$	2	$n2_{1c}$	2	$r1_{1c}$	1
$n1_{1d}$	2	$n2_{1d}$	2	$r1_{1d}$	1
$n1_{2c}$	2	$n2_{2c}$	2	$r1_{2c}$	1
$n1_{2d}$	2	$n2_{2d}$	2	$r1_{2d}$	1

Parameter	Value	Parameter	Value
$H_{1c,1}$	-0.016426	$H_{2c,1}$	-0.021226
$H_{1c,2}$	0.017258	$H_{2c,2}$	0.021023
$H_{1c,3}$	-4.422954	$H_{2c,3}$	0.072455
$H_{1c,4}$	4.429539	$H_{2c,4}$	-0.077897
$H_{1c,5}$	0.998398	$H_{2c,5}$	1.000766
$H_{1d,1}$	-0.014160	$H_{2d,1}$	-0.018347
$H_{1d,2}$	0.014107	$H_{2d,2}$	0.018109
$H_{1d,3}$	0.065784	$H_{2d,3}$	0.438184
$H_{1d,4}$	-0.069630	$H_{2d,4}$	-0.430225
$H_{1d,5}$	1.001037	$H_{2d,5}$	0.998227

The validation of the reduced-order model with the Aspen model for the single-phase charging state is shown in Figure S1. Overall, there is a good agreement of the output voltage from the two models for all four cell states.

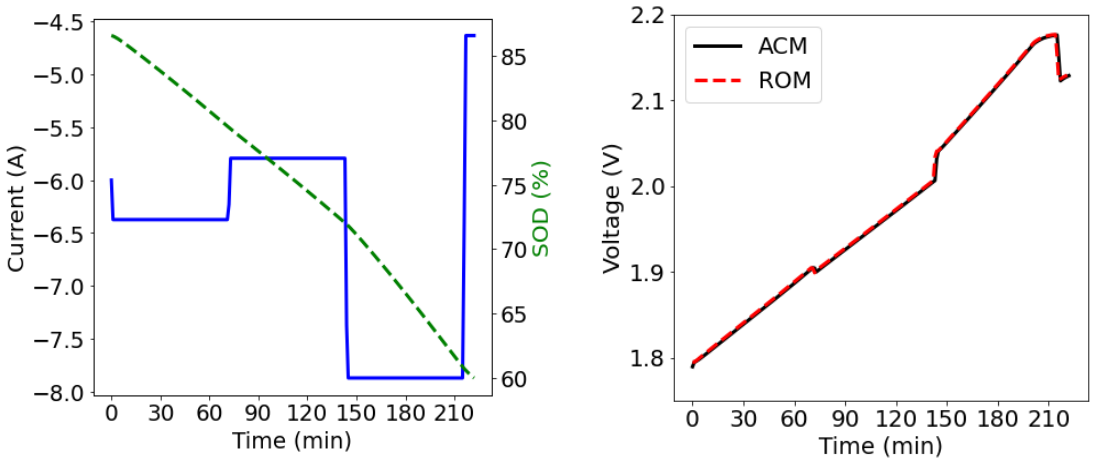

(a) (b)

Figure S1: Validation of the reduced-order model (ROM) of the NaS cell with the model from Aspen Custom Modeler (ACM) for single-phase charging state. The input data is shown in (a), with the current value varied between 4.5 A and 8 A through step changes. The variation of SOD from 86.5% to the threshold SOD is in the form of a linearly decreasing function. The corresponding output voltage data predicted by the ROM and the actual voltage data from the ACM are shown in (b). We observe that the voltage increases with decreasing SOD and the NAARX-based ROM is an accurate predictor of the actual voltage data.

S2 Battery Reduced-Order Models

S2.1 Li-ion Battery Model

From the Rint model, the terminal cell voltage V_t^{cell} (in V) is represented by Eq. 7a. For Li-ion batteries, the OCV is a nonlinear function of the SOC/SOD. This OCV-SOC characteristic curve is modeled using a fitted polynomial function given by Eq. 7b for a temperature of 25 °C.[2] We define $is \in \mathcal{S}^{'} = \{charge, discharge\}$ to denote the set of cell states representing charging and discharging. $f_{is,t}$ in Eq. 7a denotes the flag variable for cell state is at time t, and x_t^{idle} signifies the binary variable for the idle state of the cell at time t. When the cell is in the idle state, i.e. it is neither charging nor discharging, x_t^{idle} is 1, and 0 otherwise. The flag variable helps to determine if the cell is charging or discharging at time t. For instance, if the cell is charging, i.e. the charging power yc_t (in W) is positive and the discharging power yd_t (in W) has a value of 0, $f_{charge,t}$ will be 1 and $f_{discharge,t}$ will be 0 from Eqs. 7c and 7d. For discharging, yd_t will be positive and yc_t will be 0, thereby assigning values of 0 and 1 to $f_{charge,t}$ and $f_{discharge,t}$ respectively. The current I_t^{cell} is always a positive value. Thus, from Eq. 7a, the terminal voltage increases during charging operation and reduces during discharging.

The total cell power output at time t, P_t^{cell} (in W), is represented as the difference between the

discharging and charging variables yd_t and yc_t using Eq. 7e, which makes the cell power output positive for discharging and negative for charging operation. The magnitude of the power output is determined as the product of the cell voltage and the current through the cell as given by Eq. 7f. For idle state of the cell ($x_t^{idle} = 1$), the power charged/discharged by the cell is zero, giving $yd_t = yc_t$. Eq. 7g then determines the total number of cells in the battery pack, N^{cell}, as a function of the nominal power capacity of a single cell, $nc^{po,cell}$ (in W), and the nominal power capacity nc^p of the battery (in MW). Eq. 7h establishes the relation of the nominal energy capacity nc^e (in MWh) to the nominal power capacity through the maximum storage duration, nc^h. Eq. 7i represents the power output from the battery at any given time P_t^{bat} (in MW) as a function of the power output from a single cell and the total number of cells in the battery pack. Similarly, from Eq. 7j, the total energy capacity of the battery system E_t^{bat} at any given time (in MWh) is determined as a function of the nominal energy capacity of the battery pack and the cell state of charge. Since the power equation does not include the storage round-trip efficiency, it is accounted for in the overall energy balance equation given by Eq. 7k using a fixed round-trip efficiency η^S of 95%. The upper bound on the nominal power capacity nc^p is 100 MW.

$$V_t^{cell} = OCV_t^{cell} - I_t^{cell} R^{cell}(-f_{charge,t} + f_{discharge,t})(1 - x_t^{idle}), \qquad \forall t \in \mathcal{T} \qquad (7a)$$

$$OCV_t^{cell} = a1\ {SOC_t}^3 + a2\ {SOC_t}^2 + a3\ SOC_t + a4, \qquad \forall t \in \mathcal{T} \qquad (7b)$$

$$f_{discharge,t} = \frac{1 + \frac{yd_t - yc_t}{\sqrt{(yd_t - yc_t)^2}}}{2}, \qquad \forall t \in \mathcal{T} \qquad (7c)$$

$$f_{charge,t} = \frac{1 - \frac{yd_t - yc_t}{\sqrt{(yd_t - yc_t)^2}}}{2}, \qquad \forall t \in \mathcal{T} \qquad (7d)$$

$$P_t^{cell} = yd_t - yc_t, \qquad \forall t \in \mathcal{T} \qquad (7e)$$

$$\sqrt{(P_t^{cell})^2} = V_t^{cell} I_t^{cell}(1 - x_t^{idle}), \qquad \forall t \in \mathcal{T} \qquad (7f)$$

$$N^{cell} = \frac{nc^p\ 10^6}{nc^{po,cell}}, \qquad \forall t \in \mathcal{T} \qquad (7g)$$

$$nc^e = nc^p nc^h, \qquad \forall t \in \mathcal{T} \qquad (7h)$$

$$P_t^{bat} = P_t^{cell} N^{cell} 10^{-6}, \qquad \forall t \in \mathcal{T} \qquad (7i)$$

$$E_t^{bat} = nc^e SOC_t, \qquad \forall t \in \mathcal{T} \qquad (7j)$$

$$E_{t+1}^{bat} = E_t^{bat} - (\eta^S f_{charge,t} + f_{discharge,t}) P_t^{bat} \Delta t, \qquad \forall t \in \mathcal{T} \setminus \{NT + 1\}, \qquad (7k)$$

$$0 \leq f_{is,t} \leq 1, \qquad \forall is \in \mathcal{S}'. \qquad (7l)$$

The modified energy balance including the self-discharge rate is given by:

$$E_{t+1}^{bat} = E_t^{bat} - (\eta^S f_{charge,t} + f_{discharge,t}) P_t^{bat} \Delta t - x_t^{idle} E_t^{bat} \frac{\varphi}{\frac{T}{\Delta t}},\ \forall t \in \mathcal{T} \setminus \{NT + 1\}, \qquad (8)$$

where, the self-discharge rate is denoted by the parameter φ. The last term of Eq 8 denotes that the self-discharge takes place when the battery is in the idle state.

The operational and cost parameter values for both the NaS and Li-ion technologies are given in Table S2. The values of the cost parameters reported are the nominal values based on the current technology status. There are several parameters which are specific to one technology alone, governed by the assumptions specific to that technology.

Table S2: Operational and cost parameters of NaS and Li-ion technologies

Parameter	Significance	Unit	NaS value	Li-ion value
V^{min}	Minimum cell voltage[2]	V	1.61	3
V^{max}	Maximum cell voltage[2]	V	2.23	4.25
V^{nom}	Nominal cell voltage[2]	V	2	3.65
I^{nom}	Nominal cell current	A	6	6
e_1	Coefficient of NaS cell energy capacity model	Wh	144.6	-
e_2	Coefficient of NaS cell energy capacity model	Wh	-162.13	-
$a1$	Coefficient of Li-ion cell OCV model[2]	-	-	0.82
$a2$	Coefficient of Li-ion cell OCV model[2]	-	-	-0.72
$a3$	Coefficient of Li-ion cell OCV model[2]	-	-	0.69
$a4$	Coefficient of Li-ion cell OCV model[2]	-	-	3.45
R^{cell}	Equivalent series resistance	Ω	-	0.0082
nc^{h}	Maximum storage duration[3]	h	-	4
nc^{po}	Maximum power output of battery module	MW	0.05	-
$nc^{po,cell}$	Maximum cell power output	W	15.46	25.5
$nc^{eo,cell}$	Maximum cell energy capacity	Wh	107	-
nc^{eo}	Maximum energy capacity of battery module	MWh	$nc^{eo,cell} M^{cell} 10^{-6}$	-
M^{cell}	No. of cells in a battery module	-	$\frac{nc^{po}\ 10^{6}}{nc^{po,cell}}$	-
$SC^{iv,bat}$	Battery installation cost per unit capacity[3–5]	$/kWh	907	320
$SC^{of,bat}$	Unit fixed O&M cost of battery system[3–5]	$/kWyr	10	3.79
$SC^{ov,bat}$	Unit variable O&M cost of battery system[3–5]	$/MWh	0.3	0.3
t^{lf}	Battery lifetime[3–5]	yr	15	6

S2.2 NaS Battery Model

To represent the reduced-order models, the set of possible states of the NaS cell is denoted by the set $\mathcal{S}$ with $s \in \mathcal{S} = \{1c, 2c, 1d, 2d\}$. Here, the states $1c, 2c, 1d$ and $2d$ represent single-phase charging, two-phase charging, single-phase discharging and two-phase discharging respectively. In addition, we define $is, is1 \in \mathcal{S}' = \{single, two, charge, discharge\}$ to denote the individual states given by the phase of the sulfur electrode, i.e. single or two-phase and the direction of power flow

from the cell, i.e. charging or discharging. The NAARX model for the NaS cell is given as follows:

$$V1_{s,t} = \sum_{z\in\mathcal{Z}}\sum_{j\in\mathcal{J}}\sum_{k\in\mathcal{K}} \left(-I^{cell}_{t-j+1}\right)^{z} H_{s,k}\; map^{n1}_{s,j}\; map^{k1}_{s,k,z,j}\; map^{p1}_{s,z}, \qquad \forall s\in\{1c,2c\}, \forall t\in\mathcal{T}, \tag{9a}$$

$$V1_{s,t} = \sum_{z\in\mathcal{Z}}\sum_{j\in\mathcal{J}}\sum_{k\in\mathcal{K}} {I^{cell}_{t-j+1}}^{z} H_{s,k}\; map^{n1}_{s,j}\; map^{k1}_{s,k,z,j}\; map^{p1}_{s,z}, \qquad \forall s\in\{1d,2d\}, \forall t\in\mathcal{T}, \tag{9b}$$

$$V2_{s,t} = \sum_{a\in\mathcal{A}}\sum_{b\in\mathcal{B}}\sum_{k\in\mathcal{K}} {SOD^{cell}_{t-b+1}}^{a} H_{s,k}\; map^{n2}_{s,b}\; map^{k2}_{s,k,a,b}\; map^{p2}_{s,a}, \qquad \forall s\in\mathcal{S}, \forall t\in\mathcal{T}, \tag{9c}$$

$$V3_{s,t} = \sum_{l\in\mathcal{L}}\sum_{g\in\mathcal{G}}\sum_{k\in\mathcal{K}} \left(V^{cell}_{t-g}\right)^{l} H_{s,k}\; map^{r1}_{s,g}\; map^{k3}_{s,k,l,g}\; map^{q1}_{s,l}, \qquad \forall s\in\mathcal{S}, \forall t\in\mathcal{T}, \tag{9d}$$

$$V_{s,t}{}' = V1_{s,t} + V2_{s,t} + V3_{s,t}, \qquad \forall s\in\mathcal{S}, \forall t\in\mathcal{T}, \tag{9e}$$

$$V^{cell}_{t} = \sum_{is\in\mathcal{S}'}\sum_{is1\in\mathcal{S}'}\sum_{s\in\mathcal{S}} f_{is,t} f_{is1,t} V_{s,t}{}' map^{s1}_{s,is,is1}(1-x^{idle}_{t}) + V^{cell}_{t-1} x^{idle}_{t}, \qquad \forall t\in\mathcal{T}, \tag{9f}$$

where, $V1_{s,t}$, $V2_{s,t}$ and $V3_{s,t}$ denote the portion of cell voltage determined as a function of the time-series values of the cell current, SOD and previous voltage respectively. The NAARX model is developed assuming positive current for discharging and negative for charging. As I^{cell}_{t} denotes the absolute value of the current, we have two separate equations for $V1_{s,t}$ for the charging states $1c$ and $2c$, and the discharging states $1d$ and $2d$, depicted by Eqs. 9a and 9b respectively. The two input time series of current and SOD, and the output time series of previously observed voltage are summed up to obtain the cell voltage at time t and state s, $V_{s,t}{}'$, as given by Eq. 9e. The overall voltage at time t, V^{cell}_{t}, is then computed depending on the actual state of the cell at time t using Eq. 9f. The various set mappings and parameters in Eqs. 9a-9f are defined in Section S1. In addition to the flag variables for charging and discharging, Eq. 9f also includes the flag variables for the single state and the two-phase state of the cell. These are further defined as follows:

$$f_{single,t} = \frac{1 + \frac{SOD^{cell}_{t} - SOD^{thres}}{\sqrt{\left(SOD^{cell}_{t} - SOD^{thres}\right)^{2}}}}{2}, \qquad \forall t\in\mathcal{T}, \tag{10a}$$

$$f_{two,t} = \frac{1 - \frac{SOD^{cell}_{t} - SOD^{thres}}{\sqrt{\left(SOD^{cell}_{t} - SOD^{thres}\right)^{2}}}}{2}, \qquad \forall t\in\mathcal{T}. \tag{10b}$$

If the state of discharge SOD^{cell}_{t} is greater than the threshold state of discharge SOD^{thres} of 55.8% for phase change, $f_{single,t}$ will have a value of 1 and $f_{two,t}$ will be 0. Conversely, for the two-phase state of the sulfur electrode, the state of discharge SOD^{cell}_{t} will be less than SOD^{thres}, resulting

in $f_{single,t}$ to be 0 and $f_{two,t}$ to be 1. If the cell is in the non-idle state ($x_t^{idle} = 0$), the cell voltage is determined by selecting the appropriate cell model depending on the actual cell state using the flag variables, as given by the first term of Eq. 9f. If the cell is in the idle state, the cell voltage is equal to the voltage at the past time step, as depicted by the second term of Eq. 9f.

The relationship between the cell state of discharge and the corresponding energy capacity at time t, E_t^{cell} (Wh), is expressed using a surrogate model given by Eq. 11a. Eq. 11b denotes the energy balance for the cell. To derive the battery power output from the cell output, we assume that each battery module has a maximum power capacity of 50 kW. The overall battery system is then comprised of a collection of such modules connected in parallel to achieve the desired power output. The power output from the battery at any given time is thereby determined as a function of the output from a single cell, the total number of cells in a module M^{cell} and the number of battery modules in a battery bank M^{bat} using Eq. 11c. Similarly, from Eq. 11d, we determine the total energy capacity of the battery system at a given time as a function of the cell capacity E_t^{cell} and the total number of cells. The nominal energy capacity and the nominal power capacity of the battery pack are determined as a function of the fixed nominal capacity of a single module and the number of modules connected in parallel, as shown by Eqs. 11e and 11f respectively.

$$E_t^{cell} = e_1 + e_2 SOD_t^{cell}, \qquad \forall t \in \mathcal{T}, \tag{11a}$$

$$E_{t+1}^{cell} = E_t^{cell} - P_t^{cell} \Delta t, \qquad \forall t \in \mathcal{T}, \tag{11b}$$

$$P_t^{bat} = P_t^{cell}\ M^{cell}\ M^{bat}\ 10^{-6}, \qquad \forall t \in \mathcal{T}, \tag{11c}$$

$$E_t^{bat} = E_t^{cell}\ M^{cell}\ M^{bat}\ 10^{-6}, \qquad \forall t \in \mathcal{T}, \tag{11d}$$

$$nc^{e} = nc^{eo}\ M^{bat}, \qquad \forall t \in \mathcal{T}, \tag{11e}$$

$$nc^{p} = nc^{po}\ M^{bat}, \qquad \forall t \in \mathcal{T}. \tag{11f}$$

S3 Optimization Model

In the optimization framework, the nominal power capacity nc^p is the design decision variable for both the NaS and the Li-ion batteries. The time-dependent operating decision variables include the battery power output yd_t (in W), the binary variable for the idle state of the battery x_t^{idle}, power output of the NGCC power plant P_t^{ng} (in MW) and the amount of electricity undersupply of the integrated system P_t^{us} (in MW). The power output from a single cell is determined as a function of the cell state of operation x_t^{idle} and the discharging power yd_t through the cell reduced-order models. This is scaled up to the power output from a battery module using the fixed number of cells in the module. The battery pack power P_t^{bat} is then determined as a function of the module power and the design power capacity of the battery pack nc^p. The combined power output from the NGCC plant P_t^{ng} and the battery pack is delivered to the grid to meet the net demand D_t, wherein the NGCC power output and the amount of power undersupply P_t^{us} are the decision variables.

The model variables in addition to the decision variables are defined as follows: TC: total cost (\$), $C^{iv,bat}$: battery investment cost (\$), $C^{of,bat}$: fixed O&M cost of battery (\$), $C_t^{ov,bat}$: variable O&M cost of battery at time t (\$/h), $C_t^{ov,ng}$: NGCC variable O&M cost at time t (\$/h), $C_t^{os,i}$: electricity oversupply cost of integrated system at time t (\$/h), $C_t^{us,i}$: electricity undersupply cost of integrated system at time t (\$/h), $C_t^{rc,ng}$: NGCC cycling cost at time t (\$), P_t^{ng}: NGCC gross power output at time t (MW), P_t^{os}: power oversupply at time t (MW), P_t^{us}: power undersupply at time t (MW), $\frac{\eta_t^{ng}}{\eta^{nom,ng}}$: ratio of actual NGCC efficiency to nominal efficiency at time t.

Tables S3 and S4 present the model parameters and the cost parameters for sensitivity analysis, respectively.

Table S4: Cost parameter bounds for sensitivity analysis

Parameter	Unit	Lower bound	Upper bound (Li-ion/NaS)
$SC^{iv,bat}$	\$ per kWh	50	320/907
$SC^{of,bat}$	\$ per kWyr	1	3.79/10
$SC^{ov,ng}$	\$ per MWh	10	50
$SC^{rc,ng}$	\$ per MW	0.64	64

Table S3: Model parameters

Parameter	Significance	Unit	Value
Δt	Time resolution for decision making	h	0.1667
r^{disc}	Annual discount rate	%	8
DF	Discounting factor	-	$\frac{1}{r^{disc}}\left(1-\frac{1}{(1+r^{disc})^{tlf}}\right)$
CRF	Capital recovery factor	-	$\frac{1}{DF}$
T	Time horizon in consideration	h	24
NT	Number of decision stages in time horizon	-	$\frac{T}{\Delta t}$
$SC^{ov,ng}$	Unit variable O&M cost of NGCC plant [6]	$ per MWh	30
$SC^{os,i}$	Specific oversupply penalty of integrated system [7]	$ per MWh	155
$SC^{us,i}$	Specific undersupply penalty of integrated system [7]	$ per MWh	1000
$SC^{rc,ng}$	Specific NGCC cycling costs [8]	$ per MW	0.64
π_t	Electricity price at time t	$ per MWh	-
D_t	Grid net electricity demand at time t [9]	MW	-
ro^{ng}	Ramp rate of NGCC plant as fraction of nominal capacity [10]	hr^{-1}	1.2
$P^{nom,ng}$	Nominal NGCC power output	MW	641
$m1$	Coefficient of NGCC partial load efficiency model	-	0.7355
$m2$	Coefficient of NGCC partial load efficiency model	-	0.284
$lf^{min,ng}$	Min load factor of NGCC plant	%	40

The optimization formulation minimizing the total cost of the integrated system is given below. The various attributes of the optimization model are defined as follows: The set $\mathcal{T}$ denotes the set of time steps in the scheduling horizon, where $t \in \mathcal{T} = \{1, 2, ..., NT, NT+1\}$ and NT represents the number of discrete decision stages. The $NT+1^{\text{th}}$ step denotes the start of the next identical time horizon. The overall MINLP model for a given power plant is composed of 5372 equations, 5519 continuous variables and 145 discrete variables. It is solved using the global solver BARON [11] v.21.1.13 in GAMS environment.

$$\min\ TC = C^{iv,bat} + C^{of,bat} + \sum_{t=1}^{NT}\left(\left(C_t^{ov,bat} + C_t^{ov,ng} + C_t^{os,i} + C_t^{us,i}\right)\Delta t + C_t^{rc,ng}\right) \tag{12a}$$

$$\text{s.t. } C^{iv,bat} = SC^{iv,bat}\ nc^{e}\ CRF\ \frac{T}{8760}\ 10^{3}, \tag{12b}$$

$$C^{of,bat} = SC^{of,bat}\ nc^{p}\ \frac{T}{8760}\ 10^{3}, \tag{12c}$$

$$C_t^{ov,bat} = SC^{ov,bat}\ (yc_t + yd_t)\ M^{cell}\ M^{bat}\ 10^{-6}, \qquad \forall t \in \mathcal{T} \tag{12d}$$

$$C_t^{ov,ng} = SC^{ov,ng}\ P_t^{ng}\frac{\eta^{nom,ng}}{\eta_t^{ng}}, \qquad \forall t \in \mathcal{T} \tag{12e}$$

$$C_t^{rc,ng} \geq SC^{rc,ng}\left(P_{t+1}^{ng} - P_t^{ng}\right), \qquad \forall t \in \mathcal{T} \setminus \{NT+1\} \qquad (12f)$$

$$C_t^{rc,ng} \geq SC^{rc,ng}\left(P_t^{ng} - P_{t+1}^{ng}\right), \qquad \forall t \in \mathcal{T} \setminus \{NT+1\} \qquad (12g)$$

$$C_t^{rc,ng} \geq 0, \qquad \forall t \in \mathcal{T} \setminus \{NT+1\} \qquad (12h)$$

$$C_t^{os,i} = SC^{os,i}\, P_t^{os}, \qquad \forall t \in \mathcal{T} \qquad (12i)$$

$$C_t^{us,i} = SC^{us,i}\, P_t^{us}, \qquad \forall t \in \mathcal{T} \qquad (12j)$$

$$D_t = P_t^{ng} + P_t^{bat} - P_t^{os} + P_t^{us}, \qquad \forall t \in \mathcal{T} \qquad (12k)$$

$$-0.1 \leq \frac{E_{NT+1}^{bat} - E_1^{bat}}{E_1^{bat}} \leq 0.1, \qquad (12l)$$

$$0 \leq yd_t \leq nc^{po,cell} \qquad \forall t \in \mathcal{T} \qquad (12m)$$

$$0 \leq yc_t \leq nc^{po,cell} \qquad \forall t \in \mathcal{T} \qquad (12n)$$

$$0 \leq E_t^{bat} \leq nc^{e}, \qquad \forall t \in \mathcal{T} \qquad (12o)$$

$$P_t^{bat} \leq nc^{p}, \qquad \forall t \in \mathcal{T} \qquad (12p)$$

$$-P_t^{bat} \leq nc^{p}, \qquad \forall t \in \mathcal{T} \qquad (12q)$$

$$-ro^{ng} P^{nom,ng} \Delta t \leq P_{t+1}^{ng} - P_t^{ng} \leq ro^{ng} P^{nom,ng} \Delta t, \qquad \forall t \in \mathcal{T} \setminus \{NT+1\} \qquad (12r)$$

$$\frac{\eta_t^{ng}}{\eta^{nom,ng}} = m1 + m2 \frac{P_t^{ng}}{P^{nom,ng}}, \qquad \forall t \in \mathcal{T} \qquad (12s)$$

$$I_t^{cell} = I^{nom}, \qquad \forall t \in \mathcal{T} \qquad (12t)$$

$$V^{min} \leq V_t^{cell} \leq V^{max}, \qquad \forall t \in \mathcal{T} \qquad (12u)$$

$$SOD^{min} \leq SOD_t^{cell} \leq SOD^{max}, \qquad \forall t \in \mathcal{T} \qquad (12v)$$

$$lf^{min,ng} P^{nom,ng} \leq P_t^{ng} \leq P^{nom,ng}, \qquad \forall t \in \mathcal{T} \qquad (12w)$$

$$0 \leq P_t^{os} \leq P^{nom,ng}, \qquad \forall t \in \mathcal{T} \qquad (12x)$$

$$0 \leq P_t^{us} \leq P^{nom,ng}, \qquad \forall t \in \mathcal{T} \qquad (12y)$$

$$0 \leq P_t^{g} \leq P^{nom,ng}, \qquad \forall t \in \mathcal{T} \qquad (12z)$$

$$M^{bat} \in \mathbb{Z}^+, nc^p \in \mathbb{R}^+, P_t^{ng} \in \mathbb{R}^+, P_t^{us} \in \mathbb{R}^+, yd_t \in \mathbb{R}^+, x_t^{idle} \in \{0,1\}.$$

The objective function of total integrated system cost given by Eq. 12a comprises of the investment cost and fixed O&M cost of the battery system as fixed cost components, given by the first and second terms respectively. The time-varying cost components, shown by the remaining terms of Eq. 12a, include: variable O&M cost of the battery, variable O&M cost of the NGCC power plant which includes the fuel cost, penalty on the oversupply and undersupply of electricity to the grid, and the cost associated with the ramping operation of the power plant.

Each of these cost components are further expressed through Eqs. 7e, 12b - 12h. Eq. 12b denotes the battery capital cost, which is first annualized using the capital recovery factor and then further scaled over the sub-yearly time horizon of interest. Similarly, the fixed O&M cost of the battery system is normalized over the sub-yearly time horizon in Eq. 12c. Eq. 12d calculates

the variable O&M cost of the battery as a function of the total power output. We denote the charging and discharging power outputs by two different non-negative continuous variables (yc_t and yd_t), and include the sum of the two variables in the variable O&M cost. This eliminates the need to introduce a binary variable at each time step to represent the mutually exclusive charging and discharging operation, and together with Eqs. 12m and 12n ensures that the battery is either charging, discharging or idle at a given time. Eq. 12e computes the variable operating cost of the NGCC plant including the effect of efficiency loss at partial load operation. The ramping cost associated with the dynamic operation of the NGCC plant is given by Eqs. 12f - 12h.

Eq. 12k represents the overall energy balance for the integrated system at each time step. Here, we introduce slack variables to relax the hard constraint on the system energy balance, with any violations penalized in the objective through Eqs. 12i and 12j. Eq. 12l imposes a cyclical constraint on the energy stored in the battery system over a day with a tolerance of 10%. The cyclical constraint ensures that each day is identical with respect to energy storage, such that there is no borrowing of energy between the days to meet the demand.

Eqs. 12m - 12q denote the bounds on the battery power output and energy capacity. Eq. 12r denotes the ramping constraint on the power plant output. The actual efficiency of the NGCC plant relative to the rated efficiency is expressed as a function of the partial load fraction using Eq. 12s. The parameters of the efficiency equation are determined using a linear fit for the partial load efficiency curve from the work of Van den Bergh and Delarue.[12] Finally, Eqs. 12t-12z signify the bounds on the cell current, voltage, state of discharge, NGCC power output, oversupply and undersupply of electricity, and power bought from the grid. The cell current at each time step is considered to be constant at the nominal cell current for both the NaS and the Li-ion battery technologies. The upper bound on the power oversupply, undersupply and the amount bought from the grid is assumed to be equal to the nominal power output of the NGCC plant.

S4 Cost and Emission Metrics

To evaluate the system cost with the battery integration, we calculate cost metrics such as the levelized cost of storage (LCOS) and the levelized cost of energy (LCOE).

The battery LCOS is given by the following expression:

$$LCOS = \frac{C^{iv,bat^*} + C^{of,bat^*} + \sum_{t=1}^{NT} C_t^{ov,bat^*} \Delta t \; + \; SC^{ov,ng} \sum_{t=1}^{NT} P_t^{ch^*} \Delta t}{\sum_{t=1}^{NT} P_t^{dis^*} \Delta t}, \tag{13}$$

where, $C^{iv,bat^*}, C^{of,bat^*}$ and C^{ov,bat^*} denote the optimal values of the scaled investment cost, the fixed O&M and the variable O&M cost of the battery respectively. The fourth term in the numerator represents the charging cost, or the cost of electricity charged into the battery system. As the battery is being charged using power derived from the NGCC plant, the unit cost of electricity is taken to be the variable operating cost of the power plant $SC^{ov,ng}$. $P_t^{ch^*}$ and $P_t^{dis^*}$ denote the magnitude of power charged into and discharged by the battery at time t respectively, where: $P_t^{ch^*} = -P_t^{bat^*}$ if the optimal battery power $P_t^{bat^*} < 0$, and 0 otherwise. Similarly, $P_t^{ch^*} = P_t^{bat^*}$ if the optimal battery power $P_t^{bat^*} > 0$, and 0 otherwise. The overall LCOS is thus reported as the sum of the total investment, O&M and charging cost of the battery system over the time horizon divided by the total discharged energy.

The system LCOE with battery integration is determined using Eq. 14. Here, $P_t^{tot^*}$ represents the total optimal power output of the integrated system at a given time t, and is given as the sum of the NGCC power plant, battery and renewable power plant outputs ($P_t^{ng^*} + P_t^{bat^*} + P_t^{ren^*}$).

$$LCOE = \frac{TC^*}{\sum_{t=1}^{NT} P_t^{tot^*} \Delta t}. \tag{14}$$

The CO_2 emission intensity, E^{CO2}, of the integrated system of NGCC power plant, renewable farm and battery is calculated using Eq. 15, where $P_t^{ren^*}$ denotes the optimal power output of the renewable farm at time t, and ϵ^{base} represents the base-case CO_2 emission intensity of the stand-alone NGCC power plant. In addition, ϵ^{bat} represents the life cycle emission intensity of the battery, and ϵ^{ren} denotes the life cycle emission intensity of the solar farm.

$$E^{CO2} = \frac{\sum_{t=1}^{NT} \left(P_t^{ng^*} \epsilon^{base} + P_t^{dis^*} \epsilon^{bat} + P_t^{ren^*} \epsilon^{ren} \right) \Delta t}{\sum_{t=1}^{NT} \left(P_t^{ng^*} + P_t^{bat^*} + P_t^{ren^*} \right) \Delta t}. \tag{15}$$

S5 Solutions

S5.1 Battery Selection Sensitivity Study

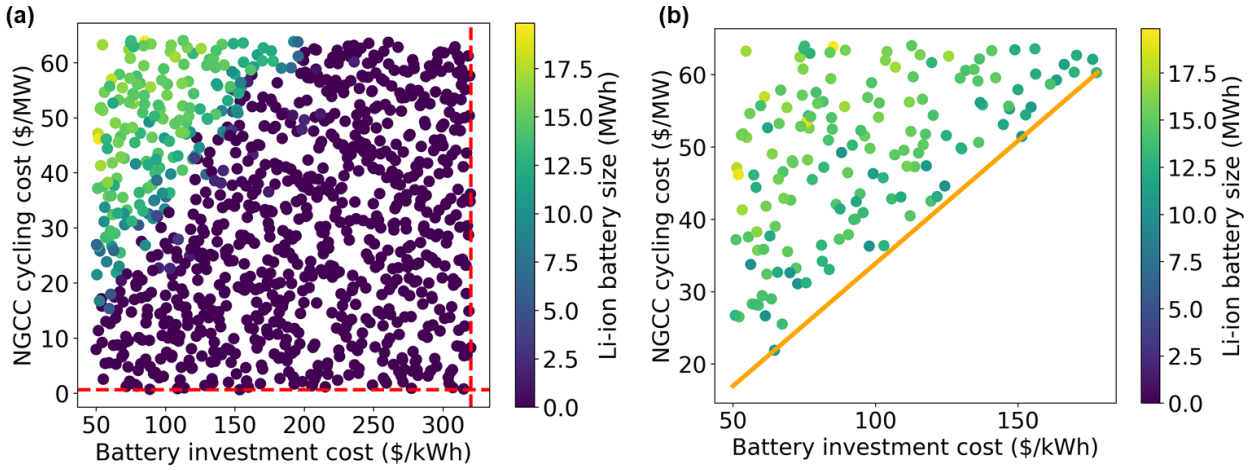

Figure S2: Sensitivity analysis of optimal Li-ion battery integration size with NGCC cycling cost and battery investment cost, where (a) shows the battery size variation for the entire range of the cost parameters, and (b) focuses specifically on the region where battery selection is optimal. The red dashed lines in (a) denote the nominal values of the cost parameters. The orange solid lines in (b) represent the threshold values of the cost parameters for battery selection.

To determine the combination of the cost parameters which favor the battery selection for the nominal net load profile, we conduct a sensitivity study of the 5 specific cost parameters: the battery installation cost, battery fixed and variable O&M cost, NGCC variable O&M cost and NGCC cycling cost, on the integration economics. The lower and upper bounds of the cost parameters considered for the analysis for both the NaS and Li-ion technologies are provided in Table S4. We generate 1000 sample points based on Latin Hypercube Sampling (LHS) design of the cost parameters between these bounds. Through this analysis, we find that the battery unit investment cost, $SC^{iv,bat}$, and the NGCC specific cycling cost, $SC^{rc,ng}$, are the two most important parameters influencing battery selection and size for both storage technologies. Figure S2 shows the variation of the optimal Li-ion battery integration size with the two crucial cost parameters. The sensitivity analysis for NaS battery is shown in Figure S3. We observe that the ratio of the NGCC specific cycling cost and the battery unit investment cost has to be greater than 0.33 for Li-ion battery and 0.27 for NaS battery to achieve favorable economics of integration with the NGCC plant. For cases where the battery is selected, the battery integration size does not exceed 20 MWh for Li-ion and 35 MWh for NaS battery. Furthermore, the average reduction in NGCC cycling costs from battery integration is 5.18% considering Li-ion integration and 4.87% with NaS integration.

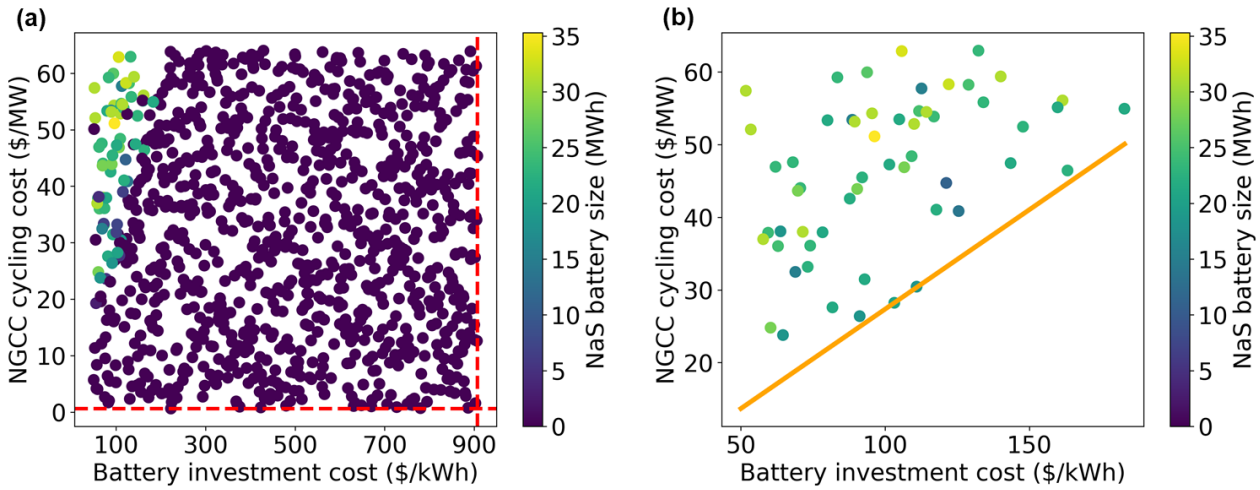

Figure S3: Sensitivity analysis for NaS battery integration size with NGCC cycling cost and battery investment cost.

S5.2 Battery Operational Profiles

The optimal operational profiles of the NGCC power plant with the Li-ion and NaS battery integration are shown in Figure S4. We observe that there is an underutilization of the battery capacity resulting from bounds imposed on the battery state and voltage for safe operation. For instance, in this case, although the optimal installed capacity of the NaS battery is 134 MW, the power discharged at any time period does not exceed 116 MW. Thus, the battery storage is overdesigned owing to the limitations on its utilization. This can also be observed from Figure S4d for the NaS battery, which shows the optimal battery operational profile. The SOD is 65% at the beginning of the day and is brought to an SOD level of 67.5% at the end of the day due to the cyclical constraint on the energy stored. The SOD hits the lower bound of 40% when the battery is charged during the afternoon hours. To avoid going below the lower bound of SOD, the entire excess energy in the afternoon hours is not stored in the battery. Similarly, the amount of energy that can be discharged is limited by the cyclical constraint. Similar operation is observed from Figure S4b for the Li-ion case. However, due to the lower storage duration compared to NaS battery, the amount of power oversupply/undersupply is higher.

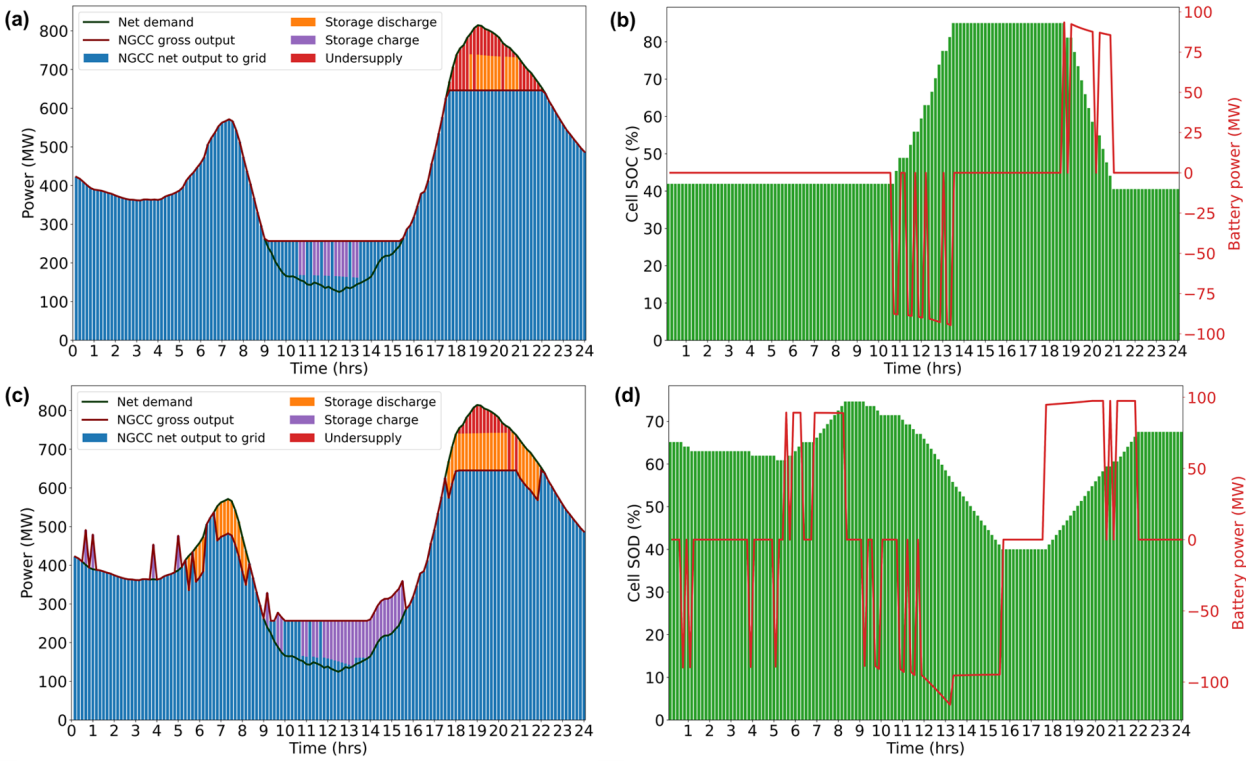

Figure S4: Optimal operational profiles for (a) integrated system comprising the power plant and Li-ion battery, (b) Li-ion battery system, (c) integrated system comprising the power plant and NaS battery and (d) NaS battery system. The profiles are shown for a time discretization of 10 minutes within a time horizon of 1 day of operation. Plots (b) and (c) show opposite trends as they represent the different state variable used in the Li-ion and NaS models: SOD and SOC, respectively.

S5.3 Variation of Battery Cost and Size for Integration with NGCC Power Plants

Figure S5 depicts the variation in the battery integration size in terms of both the energy and power capacities with increasing demand variability. For a given power plant, the increase in the battery integration size is the highest as we move from 20% to 40% increase in renewables. Additionally, for high NGCC nominal capacities, the optimal Li-ion battery size is at the upper bound of 100 MW/400 MWh.

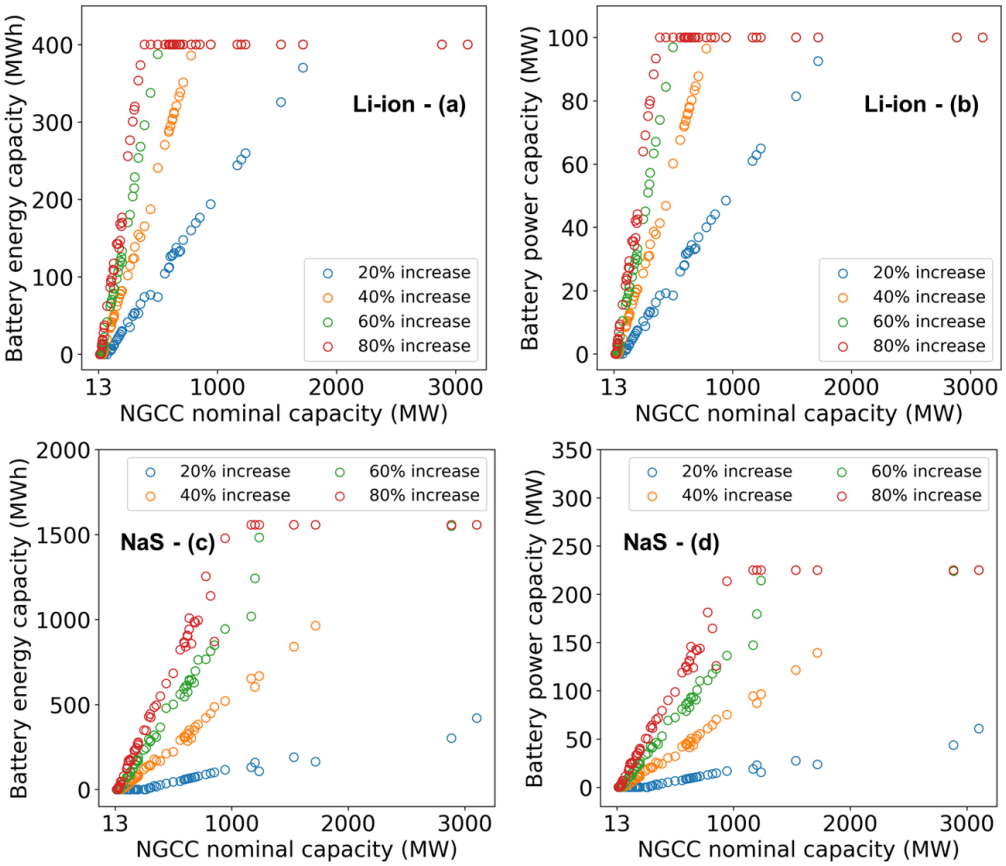

Figure S5: Optimal battery integration size in terms of (a) Li-ion nominal energy capacity, (b) Li-ion nominal power capacity, (c) NaS nominal energy capacity and (d) NaS nominal power capacity for increasing renewable penetration.

Figure S6 depicts how the different cost components constituting the overall LCOE change as we vary the extent of renewable penetration for the different power plants for the representative case of NaS battery integration. We observe that the three components majorly contributing to the overall LCOE include the battery investment cost, NGCC variable cost and the electricity undersupply cost. Among these, the battery investment cost increases with the battery size as we increase the renewable penetration and the power plant nameplate capacity. The undersupply cost also increases across the various renewable penetration scenarios. However, the average increase is not as significant as the increase in the battery cost. The increasing undersupply cost can be attributed to the peak in the net demand profile which increases as we increase the renewable penetration. Although a bigger battery can provide the required discharge power to reduce undersupply as we increase the renewable penetration, there is a trade-off between completely meeting the demand peak and the battery cost. An interesting observation from Figure S6 is that the NGCC variable operating and fuel cost decreases with increasing battery size. The NGCC cycling cost forms a small component of the LCOE and does not show a distinct trend for increasing battery size at the same renewable penetration level. The increasing battery investment and the electricity

undersupply cost with the renewable penetration and NGCC nominal capacity contributes majorly to the overall increasing trend shown by the overall LCOE.

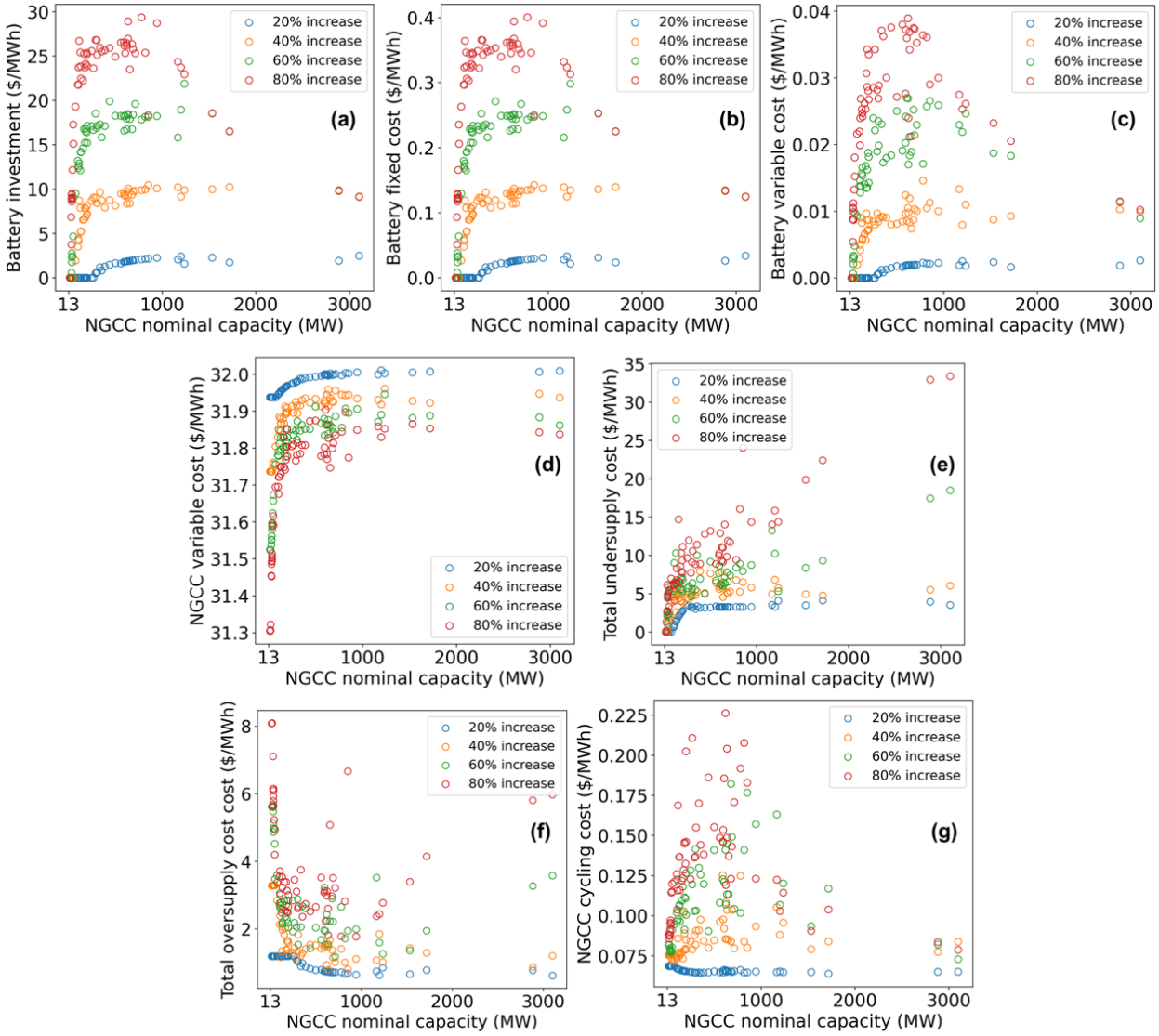

Figure S6: Cost components of (a) battery investment cost, (b) battery fixed cost, (c) battery variable cost, (d) NGCC variable cost, (e) electricity undersupply cost, (f) electricity oversupply cost and (g) NGCC cycling cost constituting the LCOE of the integrated system for 20%, 40%, 60% and 80% increase in renewable energy penetration considering NaS battery integration.

References

[1] S. Schaefer, S. P. Vudata, D. Bhattacharyya, and R. Turton, "Transient modeling and simulation of a nonisothermal sodium–sulfur cell," *Journal of Power Sources*, vol. 453, p. 227849, 2020.

[2] R. Zhang, B. Xia, B. Li, L. Cao, Y. Lai, W. Zheng, H. Wang, W. Wang, and M. Wang, "A study on the open circuit voltage and state of charge characterization of high capacity lithium-ion battery under different temperature," *Energies*, vol. 11, no. 9, p. 2408, 2018.

[3] W. Cole, A. W. Frazier, and C. Augustine, "Cost projections for utility-scale battery storage: 2021 update," tech. rep., National Renewable Energy Lab.(NREL), Golden, CO (United States), 2021.

[4] K. Mongird, V. V. Viswanathan, P. J. Balducci, M. J. E. Alam, V. Fotedar, V. S. Koritarov, and B. Hadjerioua, "Energy storage technology and cost characterization report," tech. rep., Pacific Northwest National Lab.(PNNL), Richland, WA (United States), 2019.

[5] K. Mongird, V. Viswanathan, J. Alam, C. Vartanian, V. Sprenkle, and R. Baxter, "2020 grid energy storage technology cost and performance assessment," *Energy*, 2020.

[6] U.S. Energy Information Administration, "Capital cost estimates for utility scale electricity generating plants." `https://www.eia.gov/analysis/studies/powerplants/capitalcost/`. (accessed May 2021).

[7] California ISO, "2019 annual report on market issues and performance." `http://www.caiso.com/Documents/2019AnnualReportonMarketIssuesandPerformance.pdf`. (accessed May 2021).

[8] N. Kumar, P. Besuner, S. Lefton, D. Agan, and D. Hilleman, "Power plant cycling costs," tech. rep., National Renewable Energy Lab.(NREL), Golden, CO (United States), 2012.

[9] California ISO, "Today's outlook." `http://www.caiso.com/TodaysOutlook/Pages/default.aspx`. (accessed May 2021).

[10] M. A. Gonzalez-Salazar, T. Kirsten, and L. Prchlik, "Review of the operational flexibility and emissions of gas-and coal-fired power plants in a future with growing renewables," *Renewable and Sustainable Energy Reviews*, vol. 82, pp. 1497–1513, 2018.

[11] N. V. Sahinidis, "BARON: A general purpose global optimization software package," *Journal of Global Optimization*, vol. 8, no. 2, pp. 201–205, 1996.

[12] K. Van den Bergh and E. Delarue, "Cycling of conventional power plants: technical limits and actual costs," *Energy Conversion and Management*, vol. 97, pp. 70–77, 2015.